Plasma Chem Plasma Process (2016) 36:1051–1065
DOI 10.1007/s11090-016-9707-4

ORIGINAL PAPER

Highly Sensitive Electrochemical Bioassay for Hg(II) Detection Based on Plasma-Polymerized Propargylamine and Three-Dimensional Reduced Graphene Oxide Nanocomposite

D. L. Peng[1] · H. F. Ji[1] · X. D. Dong[1] · J. F. Tian[1,2] · M. H. Wang[1] · L. H. He[1] · Z. Z. Zhang[1,2] · S. M. Fang[1,2]

Received: 12 September 2015 / Accepted: 10 April 2016 / Published online: 29 April 2016

Abstract In this study, a nanocomposite consisting of three-dimensional reduced graphene oxide (3D-rGO) and plasma-polymerized propargylamine (3D-rGO@PpPG) was prepared and used as a highly sensitive and selective DNA sensor for detecting Hg^{2+}. Given the high density of amino groups in the resultant 3D-rGO@PpPG nanocomposite, thymine-rich and Hg^{2+}-targeted DNA was preferentially immobilized on the fabricated sensor surface via the strong electrostatic interaction between DNA strands and the amino-functionalized nanocomposites, followed by detecting Hg^{2+} through T–Hg^{2+}–T coordination chemistry between DNA and Hg^{2+}. The results of electrochemical measurements revealed that the anchored amount of DNA strands anchored on the 3D-rGO@PpPG nanofilm surface affects the determination of Hg^{2+} in aqueous solution. It showed high sensitivity and selectivity toward Hg^{2+} within concentrations ranging from 0.1 to 200 nM and displayed a low detection limit of 0.02 nM. The new strategy proposed also provides high selectivity of Hg^{2+} against other interfering metal ions, good stability, and repeatability. The excellent applicability of the developed sensor confirms the potential use of plasma-modified nanofilms for the detection of heavy metal ions in real environmental samples and water.

Keywords Plasma-polymerized propargylamine · Three-dimensional reduced graphene oxide · Detection of Hg^{2+} · Electrochemical biosensor

Electronic supplementary material The online version of this article (doi:10.1007/s11090-016-9707-4) contains supplementary material, which is available to authorized users.

✉ Z. Z. Zhang
mainzhh@163.com

✉ S. M. Fang
mingfang@zzuli.edu.cn

[1] Henan Provincial Key Laboratory of Surface and Interface Science, Zhengzhou University of Light Industry, No. 166, Science Avenue, Zhengzhou 450001, People's Republic of China

[2] Henan Collaborative Innovation Center of Environmental Pollution Control and Ecological Restoration, Zhengzhou University of Light Industry, No. 166, Science Avenue, Zhengzhou 450001, People's Republic of China

Introduction

Mercury is a heavy metal ion that is highly toxic to the environment and various organisms because of its high reactivity, extreme volatility, and relative solubility in water and living tissues [1]. Even low concentrations of Hg^{2+} in organisms can cause DNA damage, inhibit ligand-receptor interactions, disable normal functions of the liver and kidney, disrupt immune system homeostasis, and even lead to death [2–4]. Therefore, methods for the sensitive and selective detection of mercury contaminants in the environment and food industry are an urgent necessity. Even various sensor systems for detecting Hg^{2+} have been reported [5–9], these sensors present certain limitations, such as poor selectivity, low sensitivity, and incompatibility with aqueous environments. Therefore, developing a more sensitive, selective, inexpensive, and environment-friendly sensor for Hg^{2+} detection is remarkably desirable. Traditional methods for Hg^{2+} detection include surface-enhanced Raman scattering [10], colorimetric and fluorescent [11], coupled to ion chromatography inductively coupled plasma mass spectrometry (ICP-MS) [12], and so on. In comparison with the conventional approaches, the electrochemical approach is one of the effective and low cost methods to detect Hg^{2+}. Electrochemical method can provide a reliable approach for detecting Hg^{2+} due to its high sensitivity, simplicity, and fast [13].

The high specificity for the interaction of oligonucleotides with metal ions prompts the oligonucleotides to be the current tools for detecting metal ions. For example, strong and stable thymine–Hg^{2+}–thymine complexes (T–Hg^{2+}–T) between DNA and Hg^{2+} have recently been applied to detect Hg^{2+} ions [14, 15]. Single-strand DNA (ss-DNA) can also fold into double-helical structures through addition of Ag^{+} to cytosine–cytosine (C–Ag^{+}–C) mismatches [16, 17]. A Pb^{2+}-induced allosteric G-quadruplex DNAzyme has also been utilized for Pb^{2+} ion detection [18–20]. To improve the adsorbed amount of oligonucleotide chains and amplify detection signals, oligonucleotide chains are often initially immobilized onto nanomaterials, nanocomposites, or polymeric films. Long et al. [21] reported a fluorescent sensor for Hg^{2+} detection based on CdS nanomaterials. Ding et al. [22] reported gold nanoparticle/graphene heterojunctions that were used as sensitive layers for Hg^{2+} detection. Liu et al. [23] also prepared a conjugated polymer-based "mix-and-detect" optical sensor for Hg^{2+} and achieved improved detection limits.

Polymer films are capable of three-dimensional network formation in aqueous solution and could supply a large number of adsorption positions for oligonucleotide immobilization [24, 25]. However, most polymers exhibit poor electrochemical performance and are seldom used as electrochemical biosensors. By contrast, a high degree of conjugation can be formed in plasma-polymerized propargylamine (PpPG) due to the formation of C=C when $C \equiv C$ bonds are irradiated by plasma discharge. It indicates that PpPG films may exhibit good electrochemical performances [26]. Owing to its unique properties such as large surface area, and electric conductivity, graphene has been widely applied in many fields, such as super-capacitors [27], energy storage [28], and biotechnology [29, 30]. However, the bonding interaction of graphene with biomolecules as well as its adsorptive capability must be improved due to its poor functionality. Actually, three-dimensional (3D) reduced graphene oxide (3D-rGO) exhibits excellent physical and chemical attributes, including a large specific surface area, excellent conductivity, and good mechanical properties [31, 32].

Combining the advantages of PpPG and 3D-rGO, a new type of electrochemical biosensor, i.e., a graphene-based nanocomposite modified using PpPG film with a high density of amino groups, may be developed. In the previous work, PpPG was deposited on the surface of graphene nanosheets and applied as the sensitive layer for the detection of

the target DNA molecules [33]. It showed a relative high detection limitation of the analyte, 1.81 nM. In comparison with 3D-rGO, the two dimensional graphene nanosheets shows the limited specific surface area, leading to the low amounts of immobilized DNA molecules. Therefore, compared with the routine method, the present work shows three advantages: (1) the loose and porous structure of 3D-rGO@PpPG nanocomposite with large specific surface areas provides a large number of active sites for attaching oligonucleotides; (2) the high density of amino groups in the developed nanocomposite can enhance the affinity between oligonucleotides and the sensing layer; and (3) the facile preparation of the nanocomposites could broaden the practicability of plasma polymers as the electrochemical biosensor. Herein, the first two advantages imply that the fabricated electrochemical biosensor could be used to detect heavy metal ions when the corresponding oligonucleotides are immobilized on the nanocomposite. In this paper, a highly sensitive electrochemical biosensor based on nanocomposite layers of 3D-rGO and PpPG for detecting Hg^{2+} in aqueous solution is reported. A schematic of the fabrication process of the sensitive DNA sensor is shown in Fig. 1. Given that the developed 3D-rGO@PpPG nanocomposite is amino group-rich and possesses high functionality, the nanocomposite contributes to the high affinity for the biomolecule adsorption of the biosensor matrix. In this research, the capabilities of DNA sensing films for detecting Hg^{2+} ions were investigated via electrochemical techniques and quartz crystal microbalance (QCM); herein, a high detection limit of 0.02 nM within the range of 0.1 to 200 nM was obtained.

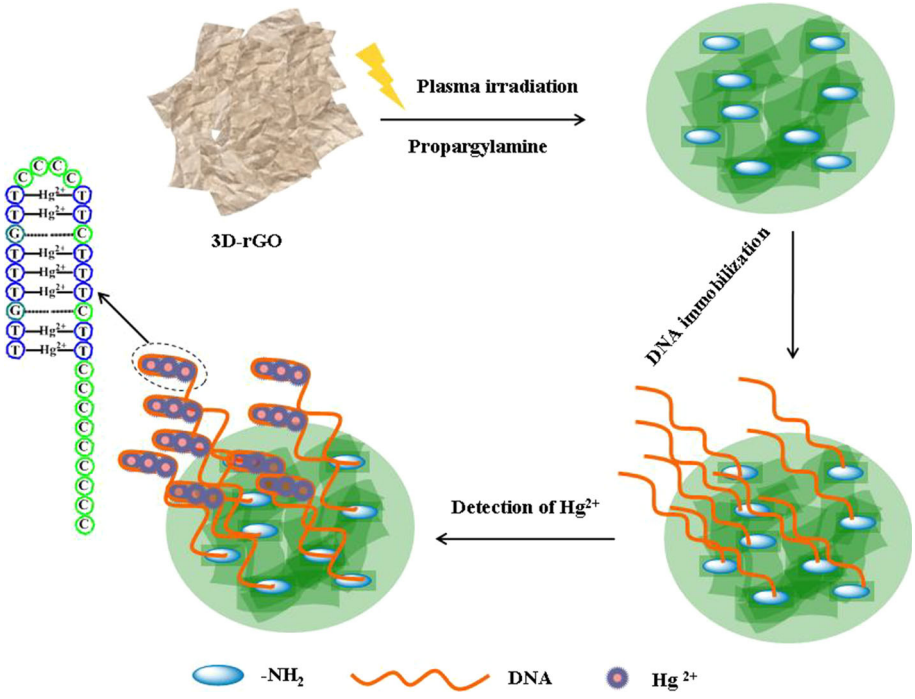

Fig. 1 Schematic of the fabricated electrochemical biosensor based on 3D-rGO@PpPG nanocomposite for detecting Hg^{2+}

Experimental

Materials and Chemicals

Propargylamine and cysteine were purchased from Aladdin Reagent (Shanghai, China). $K_3[Fe(CN)_6]$ and $K_4[Fe(CN)_6]\bullet 3H_2O$ were obtained from Sinopharm Chemical Reagent Co., Ltd. (Shanghai, China). Graphite powder (99.95 %), H_2SO_4, $KMnO_4$, H_2O_2 (30 wt %), and hydrazine hydrate(98 %) were purchased from Aladdin reagent (Shanghai, China). All other reagents used were of analytical grade and applied without further purification. DNA was obtained from SBS Genetech Co., Ltd. (Beijing, China).The sequence of the Hg^{2+}-targeted DNA was as follows: 5′-CCC CCC CCC CCC TTC TTT CTT CCC CTT GTT TGT T-3′.

Solutions

DNA solution was prepared in phosphate buffer saline (PBS, pH 7.4) composed of 0.1 M Na_2HPO_4 and 0.1 M KH_2PO_4 [$v(Na_2HPO_4):v(KH_2PO_4) = 8:2$]. The electrolyte solution was prepared immediately before use by dissolving 1.65 g of $K_3[Fe(CN)_6]$ and 2.11 g of $K_4[Fe(CN)_6]\cdot 3H_2O$ in 1 L of PBS. All solutions were prepared immediately before each experiment and stored at 4 °C until use. The Hg^{2+} stock solution (1 mM) was prepared by dissolving $Hg(NO_3)_2$ with 0.5 % of HNO_3. To evaluate the application of the proposed DNA biosensor, three samples were collected from three sewage outfalls along the Xushui River (Zhengzhou, China). These samples were diluted with equal volumes of PBS (pH 7.4) and then filtered through 0.2 μm membranes to remove impurities.

Apparatus

Fourier-transform infrared (FT-IR) spectrum was obtained by deposition of PpPG on KBr pellets coated with 3D-rGO and collected by cumulating 32 scans at a resolution of 4 from 400 to 4000 cm^{-1}. Chemical structures and components of the samples were analyzed by X-ray photoelectron spectroscopy (XPS) using a VG ESCALAB HP photoelectron spectrometer equipped with an analyzer and preparation chambers. An Al Kα ($h\nu = 1486.6$ eV) X-ray source with a power ≤100 W was used to record the spectra. Silicon wafer was used as the substrate for XPS characterization. The thickness of the plasma-polymerized films was determined by a step profiler (Alpha Step IQ of KLA Tencor Co. Ltd). To evaluate the applicability of the developed electrochemical biosensor, the real water samples were also analyzed using the proposed method and an ICP-MS Sciex Elan 5000 spectrometer (PerkinElmer, Norwalk, CT, USA).

Sensor Design

The preparation procedure of the DNA biosensor based on the 3D-rGO@PpPG nanocomposite for detecting Hg^{2+} was shown in Fig. 1. The T-rich sss-DNA was used as the probe and immobilized on the 3D-rGO@PpPG-modified Au electrode to detect Hg^{2+}. ss-DNA is composed of 2 complementary G–C base pairs and 14 mismatched C bases if folded. 7 T–Hg^{2+}–T base pairs will be formed and then cooperate to stabilize the duplex in the presence of Hg^{2+}, leading to the construction of a duplex-like DNA scaffold. The

concentration of Hg^{2+} added is directly relative to the variation of the electrochemical signal and the frequency of QCM measurements.

Pre-treatment of Silicon wafers, QCM Chips and Au Electrodes

Silicon wafer, quartz chips with 50 nm Au film, and Au electrode (3 mm in diameter) were cleaned using piranha solution (70 % H_2SO_4/30 % H_2O_2), followed by washing with Milli-Q water. As for the bare Au electrode, it also was electrochemically cleaned through a series of oxidation and reduction cycling in 0.5 M H_2SO_4 from −0.2 to 1.6 V (vs Ag/AgCl).

Modification of the QCM Chip and Au Electrode with 3D-rGO

The preparation of 3D-rGO was referred as the previous work [34]. 1.0 mg 3D-rGO was added to anhydrous ethanol and thoroughly ultra-sonicated until a homogeneous suspension of 3D-rGO was produced. Subsequently, the dispersion of 3D-rGO was spin-coated onto the silicon substrate for basic characterizations or dropped onto the surface of QCM chip and gold electrode for QCM and electrochemical measurements, respectively. The stability of 3D-rGO@PpPG nanofilm was determined by the variation of the thickness in the PBS solution using the step profiler.

Deposition of the PpPG Nanofilm on 3D-rGO-Modified QCM Chip and Au Electrode

Plasma polymerization was performed in a HQ-2 plasma enhanced chemical vapor deposition system manufactured by the Institute of Microelectronics of the Chinese Academy of Sciences, China. The schematic diagram of the plasma reactor and the electrical components is shown as Fig. S1. Propargylamine, as the monomer gas, was applied at a fixed gas flow rate of 10 sccm and constant pressure of 0.1 Torr. The PpPG films were formed on 3D-rGO-modified substrates by 13.56 Hz plasma polymerization under plasma input powers of 20, 100, and 200 W for 5 min. The substrate holder was kept at 30–50° in the reactor chamber which was detected by the digital temperature controlling system during the procedure of the plasma irradiation. The PpPG film with thickness of approximately 35 ± 3 nm was deposited onto the 3D-rGO-modified QCM chip and bare gold electrode for electrochemical and QCM measurements, respectively.

Electrochemical Measurements

QCM measurement was carried out at 9 V (direct current), for which the frequency of the vibrating quartz was determined using a Topward high-frequency counter 1220 (Topward Electric Instrument Co., Ltd., Taiwan). AT-cut, 8 MHz quartz piezoelectric crystals (Shanghai Chenhua, China) (1.2 cm diameter, 0.5 mm thickness, and Au-plated on both faces) were applied to determine the immobilization of ss-DNA and the Hg^{2+} detection. ΔF is the measured decrease in oscillation frequency.

All electrochemical measurements, including electrochemical impedance spectroscopy (EIS) and differential pulse voltammetry (DPV), were performed on a CHI660D electrochemical workstation (Shanghai Chenhua, China). A conventional three-electrode system with a gold electrode with a diameter of 3 mm as working electrode, an Ag/AgCl

(saturated KCl) electrode as the reference electrode, and a platinum slide as the counter-electrode, is used. EIS spectra were obtained in 0.5 mM $[Fe(CN)_6]^{3-/4-}$ containing 0.1 M KCl (EIS parameters: potential, 0.21 V; frequency range, 100 kHz–0.1 Hz; amplitude, 5 mV). To detect Hg^{2+}, the 3D-rGO@PpPG-modified electrode was incubated in PBS containing different concentrations of Hg^{2+} for 1 h at least, followed by rinsing with PBS. The spectrum was analyzed using Zview2 software, which utilizes nonlinear least-squares fitting to determine the parameters of the elements in the equivalent circuit. DPV data were obtained at the following condition: the potential range between 0 and 0.8 V, pulse amplitude 40 mV, step potential 3 mV, sampling width 0.00833, pulse width 0.05 s.

Results and Discussion

Optimization of Plasma Conditions for the Preparation of the 3D-rGO@PpPG Nanocomposite

QCM is a sensitive mass sensor in which an increase in mass on the quartz surface causes a decrease in the oscillation frequency of the crystal [35]. Herein, QCM kinetics was performed to determine the adsorbed amount of ss-DNA on 3D-rGO@PpPG nanofilms deposited at 20, 100, and 200 W in situ (Fig. 2a). It showed ss-DNA immobilization on all samples reached equilibrium within 40 min after the DNA solution was circulated into the flow cell until reaching stabilization. Afterwards, PBS was circulated into the system to remove unbound DNA molecules from the film surface. The ΔF values of DNA immobilized onto the 3D-rGO@PpPG films deposited at 20, 100, and 200 W were 206.8, 141.6, and 172.1 Hz, respectively. It demonstrates that DNA molecules appeared to preferentially adsorb onto the 3D-rGO@PpPG nanofilm deposited under low plasma input power, 20 W. Since high content of nitrogen, 17.5 % (Table S1), was observed in the prepared nanofilm deposited at low input power, indicating the high intensity of $-NH_2$ groups. This result was agreement with that of the G-PpPG nanofilm [33]. Thus, the strong electrostatic interaction between the negative charged phosphate groups on DNA and the positive charged amino groups of the prepared nanocomposite takes place, resulting in much more DNA strands

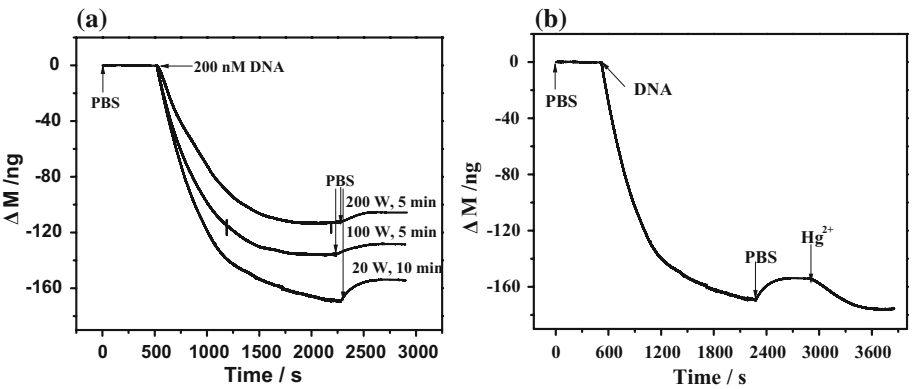

Fig. 2 **a** Kinetic curves of DNA immobilization on 3D-rGO@PpPG films deposited at 20, 100, and 200 W, as measured by QCM in situ. **b** Frequency response profiles for 200 nM Hg^{2+} deposited under a plasma input power of 20 W

anchored onto the 3D-rGO@PpPG film. As shown in Fig. 2b, probe DNA-modified 3D-rGO@PpPG film deposited at 20 W for 5 min was used as a sensing layer to detect Hg^{2+}. When 200 nM Hg^{2+} was added to the flow cell of the quartz chip, a ΔF obtained is only 21.5 Hz. It is mainly due to the coordination of probe DNA with Hg^{2+}.

Detection of Hg^{2+} Ions Using the Developed Electrochemical Sensors

EIS spectra were analyzed by Zview2 software, which uses nonlinear least-squares fitting to determine the parameters of the elements in the equivalent circuit (Inset of Fig. 3a). The circuit, which is often used to model interfacial phenomena, includes the following elements: (1) R_s, the ohmic resistance of the electrolyte solution; (2) W_o, the Warburg impedance, which results from the diffusion of ions from the bulk electrolyte to the electrode interface; (3) a constant phase element between an electrode and a solution, which corresponds to the surface condition of the electrode [33, 36]; and (4) R_{ct}, the electron transfer resistance, which exists if a redox probe is present in the electrolyte solution [37]. Figure 3a–c show the EIS spectra of the composite electrodes at various stages of Hg^{2+} detection based on three kinds of films, i.e., 3D-rGO, PpPG, and 3D-

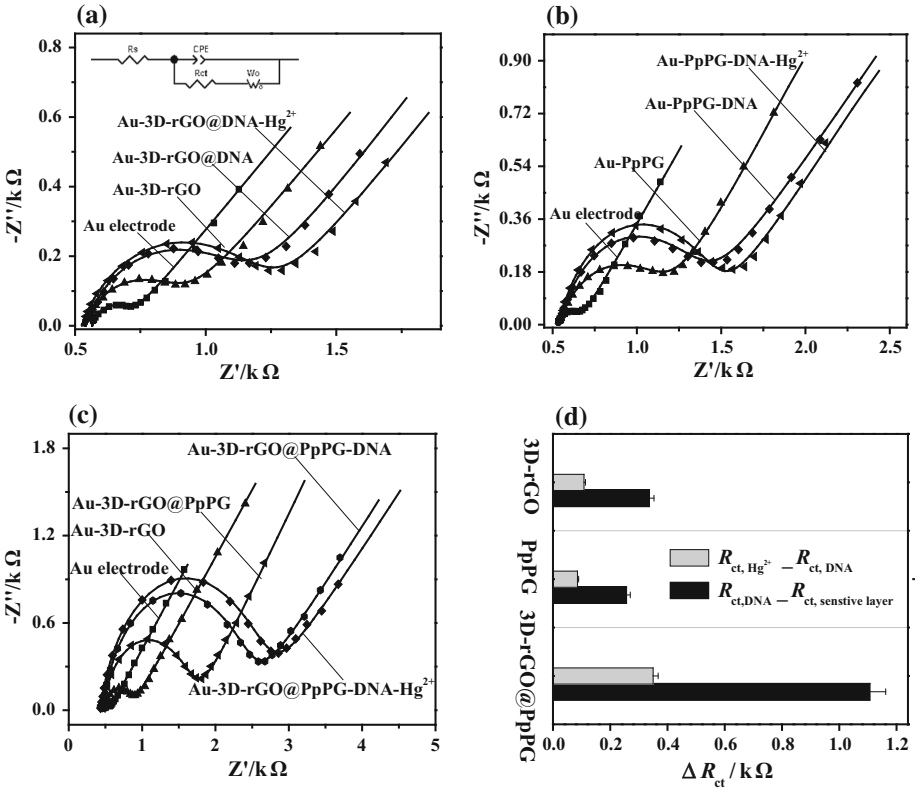

Fig. 3 EIS Nyquist plots of each stage of Hg^{2+} detection based on the fabricated electrochemical biosensors of **a** 3D-rGO, **b** PpPG, and **c** 3D-rGO@PpPG nanocomposite in 5 mM $K_3[Fe(CN)_6]$/$K_4[Fe(CN)_6]$ (1:1) and PBS (pH 7.4, containing 0.1 M KCl) from 0.01 Hz to 100 kHz with 5 mV amplitude. **d** Differences in R_{ct} values at each stage of detection for the three sensors

rGO@PpPG films. Similar trends during the composite electrode processing, ss-DNA immobilization, and Hg^{2+} detection were observed in all three cases. After the developed nanocomposite was composed with the bare gold electrode, the R_{ct} values increased, suggesting that the generated nanocomposite on the bare gold layers reduce the charge transfer efficiency. When DNA was immobilized onto the surface of the prepared nanocomposite, the repulsive interaction was formed between the negative charged phosphate of DNA and the redox couple of $Fe(CN)_6^{3-/4-}$, leading to the inhibition of the electrons access to the modified surface and the transfer efficiency in the system [38]. Since Hg^{2+} can stabilize the DNA duplex containing mismatched T–T base pair via the formation of a T–Hg^{2+}–T complex, thus resulting in an increase diameter of semicircle after the addition of Hg^{2+} [39].

To evaluate the efficiency of different sensing layers toward Hg^{2+} detection, the simulated R_{ct} values during the procedure of the Hg^{2+} detection are summarized in Fig. 3d. Differences in R_{ct} values before and after generation of a new layer adhesive (ΔR_{ct}) can represent relative bonding amounts [40]. The respective ΔR_{ct} value of 0.336, 0.257, and 1.107 kΩ for the fabricated electrochemical biosensors based on 3D-rGO, PpPG, and 3D-rGO@PpPG films were observed after DNA immobilization [41]. After DNA strands were coordinated with Hg^{2+} ions, the ΔR_{ct} ($\Delta R^{2+}_{ct,Hg}$–$\Delta R_{ct,DNA}$) value of the developed 3D-rGO@PpPG film biosensor is highest among the three cases.

Sensitivity of Hg^{2+} Determination by DPV

The sensitivity of the developed DNA sensor for detecting Hg^{2+} was determined by DPV measurements (Fig. 4a). It demonstrates the DPV curves of 200 nM 3D-rGO@PpPG-Hg^{2+} films in 0.1–200 nM Hg^{2+} ion solutions. In the presence of Hg^{2+}, evident increases in the peak current intensity of the DNA-modified 3D-rGO@PpPG films may be observed. This increase is mainly due to strong coordination interactions through the T–Hg^{2+}–T complex. As shown in Fig. 4b, a linear dependence between peak current and the logarithm of Hg^{2+} concentration was observed from 0.1 to 200 nM. The regression equation obtained was $\Delta I = 22.48 + 14.02\ \log C^{2+}_{Hg}$ with a coefficient of 0.994. The limit of detection (LOD) obtained using this method was 0.02 nM at a signal-to-noise ratio of 3. This result

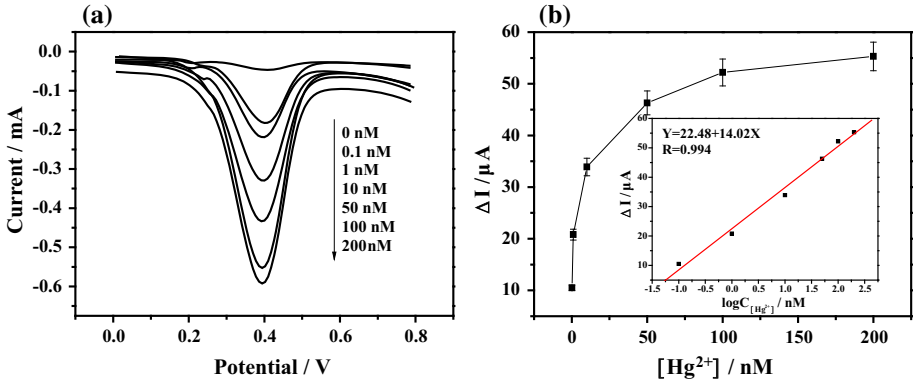

Fig. 4 **a** DPV curves of DNA-modified 3D-rGO@PpPG nanocomposite upon the addition of different concentrations of Hg^{2+} ions with the range from 0.1 to 200 nM. **b** Plot of the difference in peak current against Hg^{2+} concentration [*inset* linear calibration curve for ΔI vs. log (C^{2+}_{Hg})]

demonstrates that the linear range and LOD of the proposed sensor are comparable with those of previously reported sensing layers for Hg^{2+} detection (Table 1). In addition to the low detection limit, our strategy supplies the potential applications of plasma modified nanomaterial in the environment determination or the quality control of water.

Chemical Structures and Components of 3D-rGO@PpPG Before and After Hg^{2+} Detection

The chemical composition of the 3D-rGO@PpPG film deposited under 20 W for 5 min was investigated using FTIR, in which the relative high intensity of amino-related group in the 3D-rGO@PpPG nanocomposite was reserved (Fig. S2). The result shows the adsorption band at $\sim$3360 cm^{-1} corresponds to nitrogen-related groups, such as amino, imine, and amide bonds. The peak at $\sim$1650 cm^{-1} is assigned to the bending vibrations of N–H or the stretching vibrations of the C=C or C=N groups, whereas multiple adsorption bands at $\sim$2960, $\sim$2940, and $\sim$2880 cm^{-1} were assigned to $–CH_x$.

Additionally, XPS technique was used to characterize the variation of the surface chemical property [36, 42] during the procedure of the sensing layer fabrication for Hg^{2+} detection. The XPS survey spectra of samples were shown in Fig. S3, in which the peaks located at the binding energies (BEs) of $\sim$284.8, $\sim$400.4 and $\sim$533.0 eV are assigned to C 1s, N 1s and O 1s core-level XPS peaks in all samples, respectively. After the Hg^{2+}-targeted DNA was immobilized on 3D-rGO@PpPG surface, an additional weak peak at the BE of $\sim$133.6 eV was appeared, which is due to the presence of P 2p [50]. When detecting Hg^{2+} using the developed biosensor based on the 3D-rGO@PpPG nanocomposite, a new peak at the BE of $\sim$101.6 eV was observed, indicating the presence of Hg 4f [51]. Furthermore, the atomic % of all samples at different stages is summarized in Table S1, which can reveal the variation of the elements in samples during the fabrication the biosensor based on 3D-rGO@PpPG. After DNA was immobilization on the nanocomposite surface, C 1s and N 1s decrease in together, which could be explained by the participation of O and N in DNA molecules. Moreover, 0.49 % of Hg 4f was detected when the resultant biosensor was used to detect Hg^{2+} in aqueous solution.

Curves fitted to the C 1s, N 1s, O 1s, P 2p, and Hg 4f features of three samples at different stages during the period of Hg^{2+} detection are summarized in Fig. 5. The curve fitted to the C 1s feature is composed of four components. It reveals the presence of

Table 1 Comparison of the sensitivities of different Hg^{2+} polymeric assay methods

Sensitive layer	Detection technique	Linear range (nM)	LOD (nM)	Refs
AuNPs	Chemiluminescence	0.1–10	0.05	[45]
Self-assembled DNA layer	SWV	0.01–100	0.01	[46]
Aptamer along with Au-NPs	QCM	0.5–100	0.24	[47]
Au-NPs–rGO	Surface-enhanced Raman scattering	0.1–6000	0.1	[22]
MWCNTs and Au-NPs	DPV	0.1–20	0.03	[48]
rGO-plasma polymerized allylamine	QCM and DPV	0.1–100	0.031 and 0.017	[49]
This work	DPV	0.1–200	0.02	

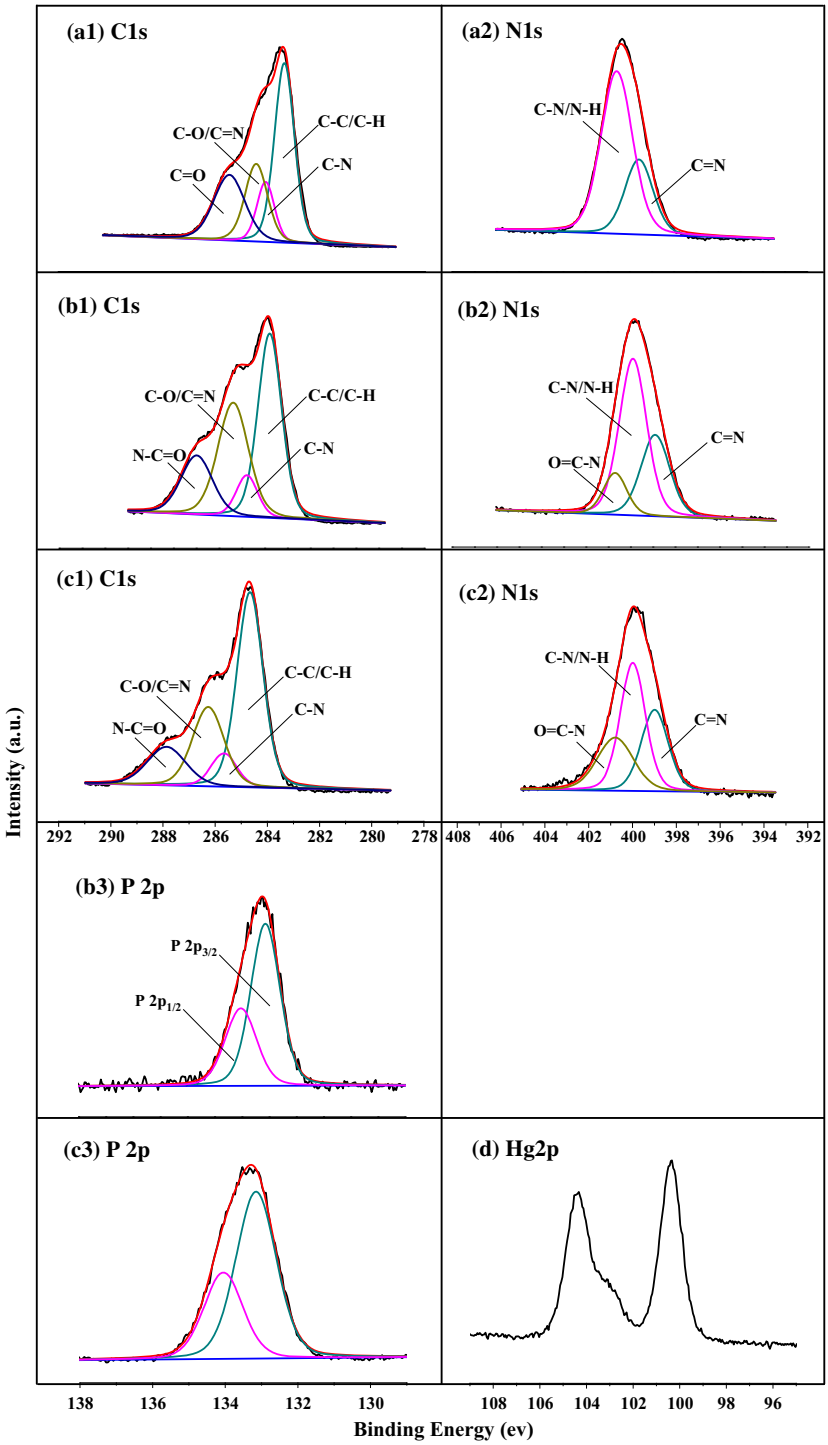
(a1) C1s
C-O/C=N
C=O
C-C/C-H
C-N
(a2) N1s
C-N/N-H
C=N
(b1) C1s
C-O/C=N
N-C=O
C-C/C-H
C-N
(b2) N1s
C-N/N-H
O=C-N
C=N
(c1) C1s
C-O/C=N
N-C=O
C-C/C-H
C-N
(c2) N1s
C-N/N-H
O=C-N
C=N
Intensity (a.u.)
292 290 288 286 284 282 280 278
408 406 404 402 400 398 396 394 392
(b3) P 2p
P 2p3/2
P 2p1/2
(c3) P 2p
(d) Hg2p
138 136 134 132 130
108 106 104 102 100 98 96
Binding Energy (ev)

◀**Fig. 5** C 1s, N 1s, P 2p, and Hg 4f core-level XPS spectra of samples at different steps during the detection of Hg^{2+} ions, i.e., 3D-rGO@PpPG, 3D-rGO@PpPG-DNA, and 3D-rGO@PpPG-DNA-Hg^{2+} sensor

hydrocarbons (C–C/C = C/C–H) at ~284.6 eV (Figs. 5a1, b1, c1) [43]; the formation of C=C was due to the decomposition of C≡C bonds contained in the monomer. Additionally, the peaks at ~285.7 and ~286.2 eV were assigned to C–N and C–O/C=N, respectively. The observation of C–N resulted from amine groups contained in the molecular chains of PpPG, whereas C=N groups were caused by the dehydrogenization of C–N groups under irradiation by the plasma discharge [52, 53]. An additional peak at ~287.6 eV was attributed to C=O groups of the as-prepared 3D-rGO@PpPG nanofilms [52]. It clearly indicates that the presence of C–O and C=O groups mainly originated from the oxidation of the rGO or molecular chains of PpPG under plasma irradiation. The presence of amine groups was confirmed by the curve fitting of the N 1s feature as shown in Figs. 5a2, b2, c2. Two peaks at ~398.8 and ~399.8 eV of the 3D-rGO@PpPG nanofilm were obtained and are due to C–N/N–H and C=N groups, respectively [54, 55]. After the ss-DNA immobilization, however, an additional peak at ~ 400.3 eV was obtained in Fig. 5b2, c2, indicating the presence of N–C=O groups. It hints at the anchoring of the ss-DNA on the amine-functionalized 3D-rGO@PpPG nanofilms.

Meanwhile, P 2p core-level XPS spectra were obtained after the DNA immobilization (Figs. 5b3, c3), in which two peaks at ~133.1 and ~134.0 eV were separated. They are assigned to P $2p_{3/2}$ and P $2p_{1/2}$, respectively [56]. When the developed biosensor was used to detect Hg^{2+} in aqueous solution, a substantial Hg 4f core-level XPS spectrum was observed (Fig. 5d), suggesting that the prepared nanocomposite can be applied to determine Hg^{2+}.

Selectivity, Repeatability, and Stability of the Hg^{2+} Detection Based on the Developed Electrochemical Biosensor

The selectivity of the developed DNA sensor for Hg^{2+} ion detection was studied by challenging the system with possible interfering ions, such as Co^{2+}, Cu^{2+}, Mn^{2+}, Ni^{2+}, Pb^{2+}, and Zn^{2+}, in real samples. Herein, 10 μM of the interfering materials was assayed with 100 nM of the target Hg^{2+} ions using DPV. As shown in Fig. 6a, high ΔI signals toward only Hg^{2+} were obtained. More importantly, high concentration of interfering agents did not induce substantial changes in current. Therefore, the developed biosensor presents acceptable sensitivity. The repeatability of the prepared sensor was also examined (Fig. 6b). A low (<10 %) relative standard deviation for 10 × parallel detections of 200 nM Hg^{2+} ions was obtained. This finding further indicates good repeatability. The fabricated electrochemical biosensor was stored in the refrigerator at 4° to evaluate the stability. The resultant sensor was measured once a day under same conditions. No substantial change of peak currents was obtained within 2 weeks, suggesting the fabricated sensor exhibited good stability.

Assay of Hg^{2+} Concentrations in Water Samples

The applicability of the DNA biosensor was evaluated by determining Hg^{2+} in river water samples. Three samples were collected from three sewage outfalls along the Xushui River (Zhengzhou, China). These samples were diluted with equal volumes of PBS (pH 7.4) and filtered through 0.2 μm membranes to remove impurities. The samples were then analyzed

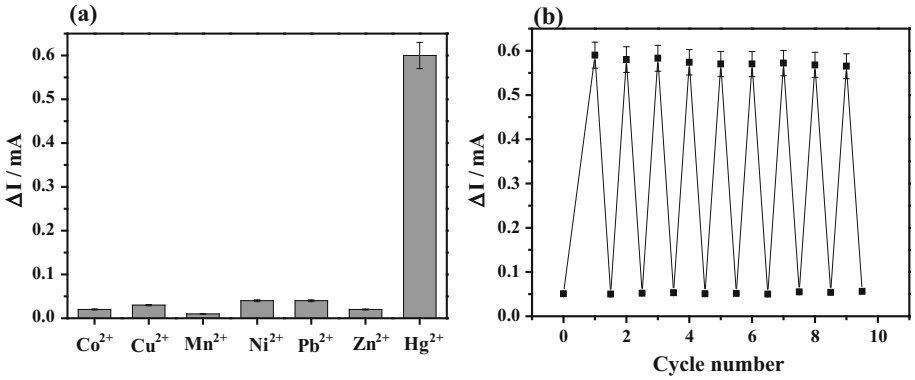

Fig. 6 **a** Changes in current in the presence of 10 μM of other metal ions and 100 nM Hg^{2+}. **b** Reusability of the DNA sensor challenged with 200 nM Hg^{2+} and washed with 10 mM cysteine

Table 2 Determination of Hg^{2+} in water samples using the proposed DNA biosensor and ICP-MS

Water sample	DNA biosensor (nM)	ICP-MS method (nM)	Relative standard deviation (%)
1	28.26 ± 3.45	30.12 ± 3.21	−6.17
2	45.74 ± 6.67	43.56 ± 4.25	5.01
3	15.53 ± 3.12	16.57 ± 1.78	−6.27

using the proposed method and ICP-MS. Results summarized in Table 2 show good agreement between the methods.

Conclusions

A novel electrochemical biosensor for detecting Hg^{2+} based on a nanocomposite of 3D-rGO functionalized by the plasma polymerization method was evaluated using electrochemical measurements. In the presence of Hg^{2+}, T-rich ss-DNA can be manipulated to form a T–Hg^{2+}–T complex. The LOD of Hg^{2+} ion was 0.02 nM. Excellent selectivity in the presence of interfering metal ions such as Co^{2+}, Cu^{2+}, Fe^{3+}, Mg^{2+}, Ni^{2+}, Pb^{2+}, and Zn^{2+} was also achieved. Hence, the as-prepared DNA sensor based on nanocomposite 3D-rGO@PpPG films may be regarded as an optional scheme for determining heavy metal ions.

Acknowledgments This work was supported by Program for the National Natural Science Foundation of China (NSFC: Account No. 51173172), Science and Technology Opening Cooperation Project of Henan Province (Account No. 132106000076), and Innovative Technology Team of Henan Province.

References

1. Yoon S, Miller EW, He Q, Do PH, Chang CJ (2007) A bright and specific fluorescent sensor for mercury in water, cells, and tissue. Angew Chem Int Ed 46:6658–6661
2. Clarkson TW, Laszlo M, Myers GJ (2003) The toxicology of mercury—current exposures and clinical manifestations. New Engl J Med 349:1731–1737

3. Harris HH, Pickering IJ, George GN (2003) The chemical form of mercury in fish. Science 301:1203
4. Morel FM, Kraepiel AM, Amyot M (1998) The chemical cycle and bioaccumulation of mercury. Annu Rev Ecol Evol Syst 29:543–566
5. Caballero A, Martínez R, Lloveras V, Ratera I, Vidal-Gancedo J, Wurst K, Tárraga A, Molina P, Veciana J (2005) Highly selective chromogenic and redox or fluorescent sensors of Hg^{2+} in aqueous environment based on 1, 4-disubstituted azines. J Am Chem Soc 127:15666–15667
6. Chen P, He C (2004) A general strategy to convert the MerR family proteins into highly sensitive and selective fluorescent biosensors for metal ions. J Am Chem Soc 126:728–729
7. Coronado E, Galan-Mascaros JR, Marti-Gastaldo C, Palomares E, Durrant JR, Vilar R, Gratzel M, Nazeeruddin MK (2005) Reversible colorimetric probes for mercury sensing. J Am Chem Soc 127:12351–12356
8. Guo X, Qian X, Jia L (2004) A highly selective and sensitive fluorescent chemosensor for Hg^{2+} in neutral buffer aqueous solution. J Am Chem Soc 126:2272–2273
9. Nolan MA, Kounaves SP (1999) Microfabricated array of iridium microdisks as a substrate for direct determination of Cu^{2+} or Hg^{2+} using square-wave anodic stripping voltammetry. Anal Chem 71:3567–3573
10. Xu L, Yin H, Ma W, Kuang H, Wang L, Xu C (2015) Ultrasensitive SERS detection of mercury based on the assembled gold nanochains. Biosens Bioelectron 67:472–476
11. Angupillai S, Hwang JY, Lee JY, Rao BA, Son YA (2015) Efficient rhodamine-thiosemicarbazide-based colorimetric/fluorescent 'turn-on' chemodosimeters for the detection of Hg^{2+} in aqueous samples. Sensor Actuat B Chem 214:101–110
12. Hong YS, Rifkin E, Bouwer EJ (2011) Combination of diffusive gradient in a thin film probe and IC-ICP-MS for the simultaneous determination of CH_3Hg^+ and Hg^{2+} in Oxic Water. Environ Sci Technol 45:6429–6436
13. Liu S, Kang M, Yan F, Peng D, Yang Y, He L, Wang M, Fang S, Zhang Z (2015) Electrochemical DNA biosensor based on microspheres of cuprous oxide and nano-chitosan for Hg(II) detection. Electrochim Acta 160:64–73
14. Tanaka Y, Oda S, Yamaguchi H, Kondo Y, Kojima C, Ono A (2007) 15N-15NJ-coupling across Hg II: direct observation of Hg II-mediated TT base pairs in a DNA duplex. J Am Chem Soc 129:244–245
15. Miyake Y, Togashi H, Tashiro M, Yamaguchi H, Oda S, Kudo M, Tanaka Y, Kondo Y, Sawa R, Fujimoto T (2006) MercuryII-mediated formation of thymine-Hg II-thymine base pairs in DNA duplexes. J Am Chem Soc 128:2172–2173
16. Chang CC, Lin S, Wei SC, Chu SY, Lin CW (2012) Surface plasmon resonance detection of silver ions and cysteine using DNA intercalator-based amplification. Anal Bioanal Chem 402:2827–2835
17. Huy GD, Zhang M, Zuo P, Ye BC (2011) Multiplexed analysis of silver(I) and mercury(II) ions using oligonucletide-metal nanoparticle conjugates. Analyst 136:3289–3294
18. Li T, Dong S, Wang E (2010) A lead (II)-driven DNA molecular device for turn-on fluorescence detection of lead (II) ion with high selectivity and sensitivity. J Am Chem Soc 132:13156–13157
19. Yang X, Xu J, Tang X, Liu H, Tian D (2010) A novel electrochemical DNAzyme sensor for the amplified detection of Pb^{2+} ions. Chem Communications 46:3107–3109
20. Chen J, Zhou X, Zeng L (2013) Enzyme-free strip biosensor for amplified detection of Pb^{2+} based on a catalytic DNA circuit. Chem Commun 49:984–986
21. Long Y, Jiang D, Zhu X, Wang J, Zhou F (2009) Trace Hg^{2+} analysis via quenching of the fluorescence of a CdS-encapsulated DNA nanocomposite. Anal Chem 81:2652–2657
22. Ding X, Kong L, Wang J, Fang F, Li D, Liu J (2013) Highly sensitive SERS detection of Hg^{2+} ions in aqueous media using gold nanoparticles/graphene heterojunctions. ACS Appl Mater Interfaces 5:7072–7078
23. Liu X, Tang Y, Wang L, Zhang J, Song S, Fan C, Wang S (2007) Optical detection of mercury (II) in aqueous solutions by using conjugated polymers and label-free oligonucleotides. Adv Mater 19:1471–1474
24. Peng H, Zhang L, Soeller C, Travas-Sejdic J (2009) Conducting polymers for electrochemical DNA sensing. Biomater 30:2132–2148
25. Goddard JM, Hotchkiss J (2007) Polymer surface modification for the attachment of bioactive compounds. Prog Poly Sci 32:698–725
26. Qiu S, Gao S, Liu Lin Z, Qiu B, Chen G (2011) Electrochemical impedance spectroscopy sensor for ascorbic acid based on copper (I) catalyzed click chemistry. Biosensor Bioelectron 26:4326–4330
27. Liu C, Li F, Ma LP, Cheng HM (2010) Advanced materials for energy storage. Adv Mater 22:E28–E62
28. Pumera M (2011) Graphene-based nanomaterials for energy storage. Energy Environ Sci 4:668–674
29. Wang Y, Li Z, Wang J, Li J, Lin Y (2011) Graphene and graphene oxide: biofunctionalization and applications in biotechnology. Trends Biotech 29:205–212

30. Shao Y, Wang J, Wu H, Liu J, Aksay IA, Lin Y (2010) Graphene based electrochemical sensors and biosensors: a review. Electroanal 22:1027–1103
31. Cao X, Shi Y, Shi W, Lu G, Huang X, Yan Q, Zhang Q, Zhang H (2011) Preparation of novel 3D graphene networks for supercapacitor applications. Small 7:3163–3168
32. Xu Y, Wu Q, Sun Y, Bai H, Shi G (2010) Three-dimensional self-assembly of graphene oxide and DNA into multifunctional hydrogels. ACS Nano 4:7358–7362
33. He L, Zhang Y, Liu S, Fang S, Zhang Z (2014) A nanocomposite consisting of plasma-polymerized propargylamine and graphene for use in DNA sensing. Microchim Acta 181:1981–1989
34. Yang Y, Kang M, Fang S, Wang M, He L, Zhao J, Zhang H, Zhang Z (2015) Electrochemical biosensor based on three-dimensional reduced graphene oxide and polyaniline nanocomposite for selective detection of mercury ions. Sensor Actuator B-Chem 214:63–69
35. Marx KA (2003) Quartz crystal microbalance: a useful tool for studying thin polymer films and complex biomolecular systems at the solution-surface interface. Biomacromolecules 4:1099–1120
36. Pajkossy T (1994) Impedance of rough capacitive electrodes. J Electroanal Chem 364:111–125
37. Wang M, Wang L, Yuan H, Ji X, Sun C, Ma L, Bai Y, Li T, Li J (2004) Immunosensors based on layer-by-layer self-assembled au colloidal electrode for the electrochemical detection of antigen. Electroanalysis 16:757–764
38. Levie DR (1965) The influence of surface roughness of solid electrodes on electrochemical measurements. Electrochim Acta 10:113–130
39. Yuan Y, Gao M, Liu G, Chai Y, Wei S, Yuan R (2014) Sensitive pseudobienzyme electrocatalytic DNA biosensor for mercury(II) ion by using the autonomously assembled hemin/G-quadruplex DNAzyme nanowires for signal amplification. Anal Chim Acta 811:23–28
40. Liu S, Nie H, Jiang J, Shen G, Yu R (2009) Electrochemical sensor for mercury (II) based on conformational switch mediated by interstrand cooperative coordination. Anal Chem 81:5724–5730
41. Noorbakhsh A, Salimi A (2011) Development of DNA electrochemical biosensor based on immobilization of ssDNA on the surface of nickel oxide nanoparticles modified glassy carbon electrode. Biosensor Bioelectron 30:188–196
42. Seah M (1980) The quantitative analysis of surfaces by XPS: a review. Surf Interface Anal 2:222–239
43. Dementjev A, De Graaf A, Van de Sanden M, Maslakov K, Naumkin A, Serov A (2000) X-ray photoelectron spectroscopy reference data for identification of the C_3N_4 phase in carbon–nitrogen films. Diam Relat Mater 9:1904–1907
44. Wang P, Kang M, Sun S, Liu Q, Zhang Z, Fang S (2014) Imine-linked covalent organic framework on surface for biosensor. Chin J Inorg Chem 32:838–843
45. Cai S, Lao K, Lau C, Lu J (2011) "Turn-on" chemiluminescence sensor for the highly selective and ultrasensitive detection of Hg^{2+} ions based on interstrand cooperative coordination and catalytic formation of gold nanoparticles. Anal Chem 83:9702–9708
46. Lou X, Zhao T, Liu R, Ma J, Xiao Y (2013) Self-assembled DNA monolayer buffered dynamic ranges of mercuric electrochemical sensor. Anal Chem 85:7574–7580
47. Dong ZM, Zhao GC (2012) Quartz crystal microbalance aptasensor for sensitive detection of mercury(II) based on signal amplification with gold nanoparticles. Sensors 12:7080–7094
48. Lu X, Dong X, Zhang K, Zhang Y (2012) An ultrasensitive electrochemical mercury (II) ion biosensor based on a glassy carbon electrode modified with multi-walled carbon nanotubes and gold nanoparticles. Anal Methods 4:3326–3331
49. Wang M, Liu S, Zhang Y, Yang Y, Shi Y, He L, Fang S, Zhang Z (2014) Graphene nanostructures with plasma polymerized allylamine biosensor for selective detection of mercury ions. Sensor Actuator B-Chem 203:497–503
50. Xu JL, Khor KA (2007) Chemical analysis of silica doped hydroxyapatite biomaterials consolidated by a spark plasma sintering method. J Inorg Biochem 101:187–195
51. Guo YF, Yan NQ, Yang SJ, Liu P, Wa J, Qu Z, Jia JP (2012) Conversion of elemental mercury with a novel membrane catalytic system at low temperature. J Hazard Mater 213–214:62–70
52. Stoica A, Manakhov A, Polčák J, Ondračka P, BuršíkováV Zajíčková R, Zajíčková L, Stoica A, Manakhov A (2015) Cell proliferation on modified DLC thin films prepared by plasma enhanced chemical vapor deposition Cell proliferation on modified DLC thin films prepared by plasma enhanced chemical vapor deposition. Biointerphases 10:029520–029529
53. Manakhov A, Nečas D, Čechal J, Pavliňák D, Eliáš M, Zajíčková L (2015) Deposition of stable amine coating onto polycaprolactone nanofibers by low pressure cyclopropylamine plasma polymerization. Thin Solid Films 581:7–13
54. Manakhov A, Skládal P, Nečas D, Čechal J, Polčák J, Eliáš M, Zajíčková L (2014) Cyclopropylamine plasma polymers deposited onto quartz crystal microbalance for biosensing application. Phys Status Solidi 211:2801–2808

55. Kingshot P, Thissen H, Griesser H (2002) Effects of cloud-point grafting, chain length, and densityof PEG layers on competitive adsorption of ocular proteins. Biomaterials 23:2043–2056
56. Majumder S, Priyadarshini M, Subudhi U, Chainy GBN, Shikha V (2009) X-ray photoelectron spectroscopic investigations of modifacations in plasmid DNA after interaction with Hg nanoparticles. Appl Surf Sci 256:438–442